Eur. J. Mineral.
2012, **24**, 851–862
Published online August 2012

Paper presented at the
7th European Conference on Mineralogy and Spectroscopy,
Potsdam, September 4–7, 2011

First-principles studies of spin-state crossovers of iron in perovskite

RENATA M. WENTZCOVITCH[1,2,*], HAN HSU[1] and KOICHIRO UMEMOTO[3]

[1] Department of Chemical Engineering and Materials Science, University of Minnesota, Minnesota 55455-0132, USA
[2] Minnesota Supercomputing Institute, University of Minnesota, Minnesota 55455-0132, USA
*Corresponding author, e-mail: wentz002@umn.edu
[3] Department of Geology and Geophysics, University of Minnesota, Minneapolis, Minnesota 55455-0132, USA

Abstract: The discovery of spin crossovers in iron under pressure in ferropericlase and iron-bearing magnesium silicate perovskite, the major mineral phases of the Earth's lower mantle, ignited in the last eight years intense discussions on the nature of this phenomenon and potential effects on the state and evolution of the Earth's mantle and of the planet as a whole. The nature of spin crossover in ferropericlase is better understood, and consensus on the interpretation of experimental data has been essentially achieved. However, in perovskite numerous experiments and computations have been carried out, often giving different results or suggesting different interpretations. Perovskite is a much more challenging system to investigate for a couple of reasons: there are two types of iron, ferrous (Fe^{2+}) and ferric (Fe^{3+}), more than one site can be occupied by iron, the A and B perovskite sites (as in ABX_3), and experiments do not probe the spin state unambiguously. Calculations are also especially difficult. This type of problem has challenged condensed matter theorists for decades. In addition, novel density functional theory + Hubbard U (DFT+U) electronic structure techniques, sometimes previously untested, are being used to address this type of problem. In summary, the challenge is multi-faceted. Here we review a series of calculations that have succeeded in reproducing experimental data and have been essential for their interpretation. They used the recently developed DFT+*Usc* method where the Hubbard U is obtained self-consistently by first principles. In particular, the electric field gradients (EFGs) at the nucleus of iron and thus quadrupole splittings (QSs) have been successfully computed, making direct comparisons between measured (via Mössbauer spectroscopy) and computed QSs for various spin states possible. This strategy led to unexpected findings in $(Mg_{1-x}Fe_x)SiO_3$ and in $(Mg_{1-x}Fe_x)(Si_{1-x}Fe_x)O_3$ ($x = 0.125$): in the pressure range of the lower mantle a) ferrous iron in the A site undergoes a site change, not a spin-state change and b) in ferric iron, spin crossover happens only in the B-site.

Key-words: spin crossover, perovskite, lower mantle, quadrupole splitting, Mössbauer spectroscopy, DFT+U.

1. Introduction

The spin-state crossover of iron in ferropericlase under pressure was observed in 2003 by X-ray emission spectroscopy (XES) (Badro *et al*., 2003). This phenomenon is often also referred to as ''spin pairing transition'' or ''spin(-state) transition''. In the following year a similar crossover was also observed in iron-bearing $MgSiO_3$ perovskite by the same technique (Badro *et al*., 2004). This phenomenon had been predicted decades ago (Fyfe, 1960; Gaffney & Anderson, 1973; Ohnishi, 1978; Sherman, 1988, 1991; Sherman & Jansen, 1995; Cohen *et al*., 1997) but the pressure conditions were challenging for experiments and it took a couple of decades to observe it. Aluminum and iron bearing perovskite, and ferropericlase, $Mg_{1-x}Fe_xO$, are the most important phases of the Earth's lower mantle, comprising ~75 vol% and ~20 vol% of this region, respectively. The remaining consists of $CaSiO_3$-perovskite, according to the pyrolitic compositional model (Ringwood, 1982). Silicate perovskite transforms into another polymorph, post-perovskite, at conditions expected to occur near the D'' discontinuity in the deep lower mantle, *i.e*. 2,500 K and 125 GPa (Murakami *et al*., 2004; Oganov & Ono, 2004; Tsuchiya *et al*., 2004; Wentzcovitch *et al*., 2006). The implications of these spin crossovers for the properties of the mantle, or of the entire planet, are yet to be fully understood, but several geodynamic simulations have already incorporated spin crossovers (Bower *et al*., 2009; Matyska *et al*., 2011; Shahnas *et al*., 2011). Today, theoretical mineral physics studies are making decisive contributions to this problem. They can reliably and selectively address different issues of complex systems and are essential to interpret the data. This article reviews the main theoretical results on the spin-state crossover in perovskite, with special focus on work by our group. This is the most important and still the most controversial system. The spin-state crossover in ferropericlase has recently been reviewed in another article (Hsu *et al*., 2010a) and we only briefly mention those results to set the stage for the discussion on perovskite.

Ferrous (Fe^{2+}) and ferric (Fe^{3+}) iron in silicates and oxides have highly localized *d* electrons and electronic

DOI: 10.1127/0935-1221/2012/0024-2249
0935-1221/12/0024-2249 $ 5.40

correlation is strong. Spin changes in strongly correlated oxides and silicates under pressure has challenged electronic structure theory for several decades. The commonly used versions of density functional theory (DFT) (Hohenberg & Kohn, 1964; Kohn & Sham, 1965), such as the local density approximation (LDA) (Ceperley & Alder, 1980; Perdew & Zunger, 1981) and generalized gradient approximation (GGA) (Perdew *et al*., 1996) often fail to explain fundamental properties of materials containing strongly correlated ions, in particular their insulating character. This challenge has inspired the development of new methods for electronic structure computations of strongly correlated materials that are mature enough to address this problem today. In this paper, we offer a review of theoretical/computational studies that have been performed to date by our group on iron-bearing perovskite and analyze the performance of different approaches by contrasting results with each other and with experimental data. Results summarized here were obtained using standard DFT within the LDA and GGA, or the internally consistent DFT+U approach (Cococcioni & de Gironcoli, 2005). For a general review of the spin crossover in ferropericlase and perovskite, including experiments up to 2007–08, we refer to a recent paper by Lin & Tsuchiya (2008). Experimental information on perovskite that has become available since then and are relevant for comparison with calculations is reviewed here.

2. Spin pairing phenomenon

Our basic understanding of the spin-pairing phenomenon can be summarized as follows: the 5-fold degeneracy of the *3d* states of iron splits in a crystalline field. The nature and ordering of the new energy levels depends primarily on the atomic structure of the first coordination shell and interatomic distances between the *3d* atom and ligands. Electronic states of iron in Earth forming silicates and oxides at ambient conditions are relatively localized. In stoichiometric compounds such as FeO and Fe_2O_3, magnetic moments of iron are anti-ferromagnetically ordered (Fjellvag *et al*., 1996; Rollmann *et al*., 2004). The solid solutions of the lower mantle are not magnetically ordered. They are paramagnetic insulators. In ferropericlase and iron-bearing perovskite, the energetic order, symmetry, and occupation of iron *3d* orbitals can be understood on the basis of crystal field symmetry and Hund's rule. In octahedral sites, the most relevant site as far as spin-state changes are concerned, orbital alignments and their energy ordering are shown in Fig. 1. Ferrous iron has six *3d* electrons. In the high-spin (HS) state, five of them have spin +1/2 (up) and one has spin -1/2 (down). Their angular momentum is essentially quenched, spin orbit interaction is not important, and the total-spin quantum number, S, is equal to 2. The intermediate-spin (IS) state has four *3d* electrons with spin up and two with spin down, for a total spin $S = 1$. The low-spin (LS) state, has three electrons up, three down, and $S = 0$. Ferric iron has five *3d* electrons; the HS state has five spin up electrons, for $S = 5/2$; the IS and LS states have $S = 3/2$ and 1/2 respectively. The charge density distribution of the partially occupied *3d* electrons is non-spherical and is related to the ordering of the energy levels established by the crystalline field and the number of *3d* electrons. This non-spherical distribution distorts the first coordination shell of ligands, the so-called Jahn-Teller (J-T) effect.

In Earth forming silicates, iron is in the HS state at ambient pressure. With increasing pressure, the Fe-O bond-length decreases, the crystal field, E_c in Fig. 1, increases, and the energy splitting between d states increases. This eventually leads to a change in the occupation of these orbitals, *i.e*. the spin pairing phenomenon is characterized by a change in the occupation of the lowest d-orbitals and a change in the total spin S. How these occupations change under pressure has been controversial, in particular the existence of the IS state. In principle, spins could pair gradually, with a change of S from 2 to 1 to 0 in ferrous iron or from 5/2 to 3/2 to 1/2 in ferric iron. In fact,

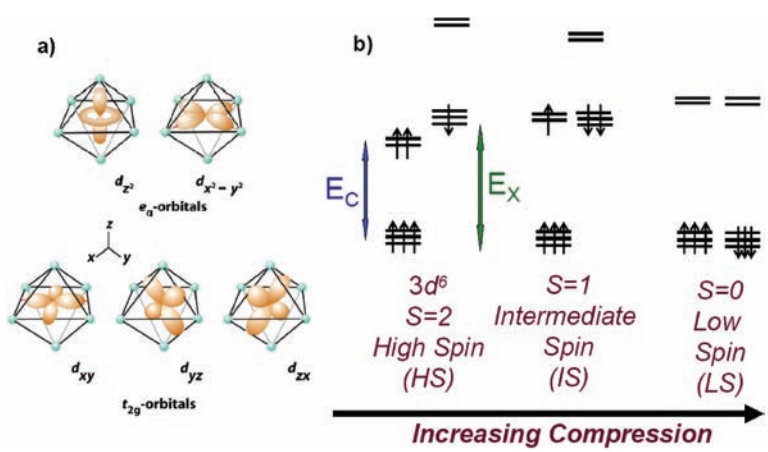

Fig. 1. (a) *3d* orbital alignments and their classification in octahedral field. E_c is the crystal field splitting and E_x is the Hund's rule energy. (b) Energy levels and occupancies for $3d^6$ ions, such as ferrous iron. Ferric iron has configuration $3d^5$ and the electron in the highest energy level is absent. Its total spin in HS, IS, and LS states are 5/2, 3/2, and ½ respectively.

the nature of these spin changes has been difficult to predict since it can depend on several factors (*e.g.*, chemistry, stoichiometry, etc). This ambiguity is illustrated very well in perovskite and it is the main reason for focusing this review on this mineral. The change in orbital occupancy is accompanied by a substantial octahedral volume reduction (Tsuchiya *et al.*, 2006) that can produce thermodynamics (Wu *et al.*, 2009), elastic, and possibly viscosity anomalies (Wentzcovitch *et al.*, 2009). This is essentially an enthalpy driven transition.

3. Theoretical approach

Iron-bearing perovskites are paramagnetic solid solutions, insulators with localized moments. Iron concentrations in the bulk lower mantle, X_{Fe}, are predicted to be relatively low ($X_{Fe} < 0.1$) (Murakami *et al.*, 2005; Irifune *et al.*, 2010). These systems are challenging to theory and computations for a couple of reasons: description of their electronic structure, treatment of their solid solutions, and calculation of their vibrational properties, without which a true thermodynamics treatment is not possible. The thermodynamics of ferropericlase has been investigated pretty extensively using an approximated model of its vibrational density of states (Wentzcovitch *et al.*, 2009; Wu *et al.*, 2009). However, perovskite is a more complex system and its theoretical investigation has not reached that same level yet.

3.1. Electronic structure methods

The strong electronic correlation in iron in mantle oxides and silicates requires use of electronic structure approaches that go beyond standard density functional theory (DFT) for predictive studies. DFT is a ''one electron'' mean-field approach (Hohenberg & Kohn, 1964; Kohn & Sham, 1965), where one solves a Schrödinger-type equation for a single electron subjected to the ''mean field'' potential created by ''all'' electrons, including the one in consideration.

$$-\frac{\hbar^2}{2m}\nabla^2\psi_i + V_{ext}(r)\psi_i + V_{el}(r)\psi_i + V_{xc}(\rho(r), \nabla\rho(r), \psi_j(r'), \nabla\psi_j(r')...)\psi_i = E_i\psi_i \quad (1)$$

In this expression $V_{ext}(r)$ is the external potential created by the ions; $V_{el}(r)$ is the electrostatic potential created by the continuous charge density created by ''all'' electrons in occupied orbitals:

$$V_{el}(r) = \int \frac{\rho(r')dr'}{|r - r'|} \quad (2)$$

where the charge density $\rho(r)$ is the summation of the charge density probability from all occupied orbitals:

$$\rho(r) = \sum_i \psi_i^*(r)\psi_i(r) \quad (3)$$

There are two issues with this electrostatic potential: (1) since ''all'' electrons are included in the calculation of the charge density, this potential includes ''self-interaction''. For delocalized states this does not present a serious problem for many properties. This is the case for most compounds without *d*- and *f*-electrons. But for systems containing localized states, such as *d*-electrons, this creates a severe problem. (2) Ultimately electrons are point charges. This departure from a continuous charge distribution is evident when electrons are localized and in close proximity, as in *d*-electrons in the same atom. This is called dynamic correlation.

$V_{xc}(\rho, \nabla\rho, \psi, \nabla\psi...)$ is the ''exchange and correlation'' potential that in principle should correct for and include all quantum correlation effects not included in $V_{el}(r)$. In the local density approximation (LDA), this potential is a local functional of the charge density, namely, $V_{xc}(\rho(r))$; in the generalized gradient approximation (GGA) it is a functional of the local charge and of the local charge gradient, $V_{xc}(\rho(r), \nabla\rho(r))$. In more complex functionals, such as meta-functionals, this potential depends on the kinetic energy, $V_{xc}(\rho, \nabla\rho, \nabla\psi)$. These are the meta-GGA or –LDA. Hybrid functionals include explicitly a certain amount of the exact exchange interaction.

The total DFT energy then is:

$$E_{DFT} = -\sum_i \frac{\hbar^2}{2m}\int \psi_i^*\nabla^2\psi_i + \int [V_{ext}(r) + V_{el}(r)]\rho(r)dr + \sum_{i,j}\int\int \psi_i^*(r)V_{xc}(\rho(r), \nabla\rho(r), \psi_j(r'), \nabla\psi_j(r')...) \psi_i(r)drdr' \quad (4)$$

Standard versions of DFT produce particularly poor structural and electronic properties for systems containing localized *d*-electrons such as ferropericlase (Tsuchiya *et al.*, 2006) and ferric iron-bearing perovskite (Hsu *et al.* 2011b). Both are predicted to be metallic, rather than insulators, by LDA or GGA. Consequently, not only electronic but also structural properties obtained with these functionals do not compare well with experiments. Hybrid- and meta-GGA type functionals, while looking promising, have not been sufficiently tested yet and are not as efficient for solid-state systems as of now. There is, however, another family of functionals, the so-called corrective functionals, to which the DFT+U method belongs (Cococcioni & de Gironcoli, 2005), that is highly efficient and has been particularly successful in describing the electronic structure of these types of systems. Other functionals in this family include, DFT+U+V, DFT+U+J, and DFT+U+V+J. These functionals have ''ad hoc'' expressions to correct directly for the known shortcomings of DFT (self-interaction and dynamic correlation). In contrast, standard DFT has described structural and elastic properties of perovskite with ferrous iron quite successfully (Kiefer *et al.*, 2002; Umemoto *et al.*, 2008; Hsu *et al.*, 2010b). They display small but non-vanishing electronic gaps, even within LDA or GGA, and orbital occupancies and charge densities are correct. The electronic

charge density is essential for describing structural properties and the introduction of the Hubbard U in the functional does not change the charge density drastically. Obviously, this is not the case for systems that are metallic in the absence of the Hubbard U. The Hubbard U, however, always affects transition pressures, since different phases, or different spin states in the same phase have different U values. This method has recently been discussed by Hsu *et al*. (2011a). Our studies of iron-bearing perovskite have tested results using the following options: LDA, LDA+U, GGA, and GGA+U. The DFT+U approach has recently been reviewed by Cococcioni (2010). In short, the total energy functional is:

$$E_{DFT+U} = E_{DFT} + \frac{U}{2}\sum_{I,\sigma} Tr\left[\mathbf{n}^{I\sigma}\left(\mathbf{1} - \mathbf{n}^{I\sigma}\right)\right] \tag{5}$$

where E_{DFT} is the DFT ground-state energy of the structure, and $\mathbf{n}^{I\sigma}$ is the occupation matrix of the atomic site I with spin σ. The atomic-like orbitals used in defining $\mathbf{n}^{I\sigma}$ are arbitrary, but the calculations of U and E are consistent with this definition (Cococcioni & de Gironcoli, 2005; Fabris *et al*., 2005). The Hubbard U is computed using linear response theory. In practice this procedure starts by computing the DFT or DFT+U (with a trial U) ground state of a given structure. The occupation matrix $\mathbf{n}^{I\sigma}$ at site I is then determined. The next step is to apply perturbations to the potential localized at the Hubbard site I. The perturbed states lead to different occupation matrices. The linear response of the occupation matrix $\mathbf{n}^{I\sigma}$ to the local potential shift is used to (re)determine the Hubbard U. In this scheme, the value of U depends on both the spin state and the unit-cell volume (Cococcioni & de Gironcoli, 2005; Tsuchiya *et al*., 2006; Hsu *et al*., 2010b, c; 2011b). U depends most strongly on valence and spin state, then on the environment, *i.e*. the structure of the first coordination shell, and then on volume.

3.2. Thermodynamic treatment of the mixed spin state

At finite temperatures, perovskite with iron concentration X_{Fe} can, in principle, have irons in multiple spin states, *i.e*. in a mixed-spin (MS) state. Knowledge of the equilibrium population of each spin state at high temperatures and pressures is crucial to study the consequences of the spin crossover on their properties. Since X_{Fe} of these minerals in actual lower-mantle perovskite is relatively small, *i.e*. < 0.10, we treat perovskite in the MS state as the ideal solid solution of the mixture of each pure spin state. This is not the same as a solid solution of, *e.g*. $MgSiO_3$ and $FeSiO_3$. The Gibbs free energy of the MS state is thus written as:

$$G(n_\sigma, P, T) = \sum_\sigma n_\sigma(P,T) G_\sigma(P,T) + G^{mix}(P,T) \tag{6}$$

where n_σ and G_σ are the fraction and Gibbs free energy of each spin state, respectively. The subscript σ denotes spin state, *i.e*. LS, IS, HS, *etc*. G^{mix} results from the entropy of mixing solution, and it is given by:

$$G^{mix} = k_B T X_{Fe} \sum_\sigma n_\sigma \log n_\sigma \tag{7}$$

The Gibbs free energy of each spin state, G_σ, has three contributions:

$$G_\sigma = G_\sigma^{stat+vib} + G_\sigma^{mag} + G_\sigma^{site} \tag{8}$$

$G_\sigma^{stat+vib}$ is the Gibbs free energy containing static and vibrational contributions. The calculation of the vibrational free energy is usually addressed using the quasiharmonic approximation (QHA) (Wallace, 1972) in combination with first principles phonons obtained using density functional theory (Baroni *et al*., 2001). In ferropericlase the QHA was used in combination with a model vibrational density of states (Wentzcovitch *et al*., 2009; Wu *et al*., 2009). In the spin crossover studies in perovskite discussed in this article, we have not included vibrational effects, since we are trying first to understand the nature of these crossovers. If this contribution is disregarded, $G_\sigma^{stat+vib}$ reduces to the static enthalpy of spin state σ,

$$G_\sigma^{stat+vib} = H_\sigma \tag{9}$$

The second term in Equation (8) derives from the magnetic entropy,

$$G_\sigma^{mag} = -k_B T X_{Fe} \log[m_\sigma(2S_\sigma + 1)] \tag{10}$$

where m_σ and S_σ are the orbital degeneracy and the spin quantum number of each spin state, respectively. The third term comes from the site entropy

$$G_\sigma^{site} = -k_B T X_{Fe} \log N_\sigma^{site} \tag{11}$$

where N_σ^{site} is the number of equivalent equilibrium sites for iron in each spin state. By minimizing the total Gibbs free energy (Equation 2) with respect to n_σ under the constraint $\sum_\sigma n_\sigma = 1$, the following expressions for each spin state are then obtained:

$$\begin{aligned} n_\sigma(P,T) = n_{HS} \times \frac{N_\sigma^{site} m_\sigma (2S_\sigma + 1)}{N_{HS}^{site} m_{HS}(2S_{HS}+1)} \\ \times \exp\left(-\frac{\Delta G_\sigma^{stat+vib}}{k_B T X_{Fe}}\right) \text{ for } \sigma \neq \text{HS} \end{aligned} \tag{12}$$

$$\begin{aligned} n_{HS}(P,T) = \left[1 + \frac{N_{LS}^{site} m_{LS}(2S_{LS}+1)}{N_{HS}^{site} m_{HS}(2S_{HS}+1)} \exp\left(-\frac{\Delta G_{LS}^{stat+vib}}{k_B T X_{Fe}}\right)\right. \\ \left. + \frac{N_{IS}^{site} m_{IS}(2S_{IS}+1)}{N_{HS}^{site} m_{HS}(2S_{HS}+1)} \exp\left(-\frac{\Delta G_{IS}^{stat+vib}}{k_B T X_{Fe}}\right)\right]^{-1} \end{aligned} \tag{13}$$

where $\Delta G_\sigma^{stat+vib} \equiv G_\sigma^{stat+vib} - G_{HS}^{stat+vib}$. Again, when the lattice vibrational contribution is disregarded, we have $\Delta G_\sigma^{stat+vib} = \Delta H_\sigma \equiv H_\sigma - H_{HS}$.

3.3. Computational details

For (Mg,Fe)SiO_3 perovskite (Umemoto *et al*., 2008, 2010; Hsu *et al*., 2010b, 2011b), computations used both LDA (Ceperley & Alder, 1980; Perdew & Zunger, 1981) and (PBE) GGA (Perdew *et al*., 1996), LDA+U and GGA+U (Cococcioni & de Gironcoli, 2005). The pseudopotentials for Fe, Si, and O were generated by Vanderbilt's method (Vanderbilt, 1990). The valence electronic configurations used were $3s^2 3p^6 3d^{6.5} 4s^1 4p^0$, $3s^2 3p^1$, and $2s^2 2p^4$ for Fe, Si, and O, respectively. The magnesium pseudopotential was generated by the method of von Barth-Car. Five configurations, $3s^2 3p^0$, $3s^1 3p^1$, $3s^1 3p^{0.5} 3d^{0.5}$, $3s^1 3p^{0.5}$, and $3s^1 3d^1$ with decreasing weights 1.5, 0.6, 0.3, 0.3, and 0.2, respectively, were used. Core radii were $r(3s) = r(3p) = r(3d) =$ 2.5 a.u. with d locality. The plane-wave cutoff energy was 40 Ry. In each supercell used, the k-point mesh is fine enough to achieve convergence within 1 mRy/Fe in the total energy. Variable-cell-shape molecular dynamics (Wentzcovitch *et al*., 1993) implemented in QUANTUM-ESPRESSO package (Giannozzi *et al.*, 2009) is used for structural optimizations. In Hsu *et al*. (2010b, 2011b), electric field gradient (EFG) tensors were calculated using the augmented plane wave + local orbitals (APW+lo) method (Madsen *et al*., 2001) implemented in the WIEN2k code (Blaha *et al*., 2001), and they are converted to the QS values using $Q = 0.16$–0.18 barn (Petrilli *et al*., 1998).

4. Spin-state crossovers in perovskite

The detailed mechanism of the spin crossover in iron-bearing magnesium silicate perovskite is still not completely understood especially the in aluminum-bearing perovskite. Much progress has been made recently by experiments and first-principles calculations but studies have not yet addressed all possibilities. The situation is considerably more complex than in ferropericlase for a couple of reasons: i) both, ferrous and ferric iron can be present; ii) while ferrous iron is believed to replace magnesium in the large A site, ferric iron can occupy both the A and/or B sites of the perovskite structure (see Fig. 2); iii) the real mantle perovskite also contains aluminum, which increases the amount of ferric iron. The percentage of ferric iron can reach 60 % (McCammon, 1997; Frost *et al*., 2004) but the uncertainty of this figure could be large; iv) experimental techniques do not reveal unambiguously the spin state. They can reveal spin state changes, or more precisely, changes in electronic configuration of iron, but not the spin state directly. For this reason, interpretation of experimental data has been difficult.

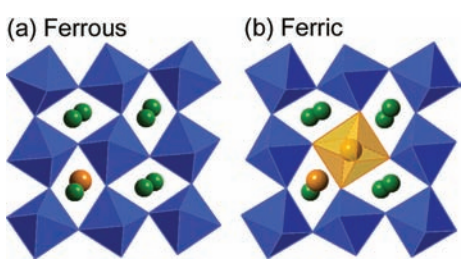

Fig. 2. Atomic structures of iron-bearing $MgSiO_3$ perovskite viewed along [001]. Yellow and green spheres represent Fe and Mg, respectively; blue and yellow octahedra represent SiO_6 and FeO_6, respectively. (a) Ferrous iron substitutes for Mg at the A site; (b) ferric iron substitute Mg at the A site and Si at the B site.

Various experimental techniques have been used to study the spin-state crossover of iron incorporated in $MgSiO_3$ perovskite, including XES (Badro *et al*., 2004; Li *et al*., 2004; Lundin *et al*., 2008; Catalli *et al*., 2010, 2011), XANES (Narygina *et al*., 2009), and Mössbauer spectroscopy (Jackson *et al*., 2005; Li *et al*., 2006; Lin *et al*., 2008; Lundin *et al*., 2008; McCammon *et al*., 2008; Grocholski *et al*., 2009; Catalli *et al*., 2010, 2011). Due to the complicated nature of iron-bearing $MgSiO_3$ perovskite (three non-equivalent iron sites), the occasional difficulty in identifying iron species in perovskite, and the lack of unambiguousness of these experimental techniques, a solid conclusion cannot be easily drawn from these experiments. For examples, the decreasing of satellite peak ($K\beta$') intensity of the XES spectra in Badro *et al*., (2004), where Fe^{2+} and Fe^{3+} coexist, was interpreted as a HS-LS crossover occurring in Fe^{2+} residing at the A site. In Li *et al*. (2004), both $(Mg_{0.87}Fe_{0.09})(Si_{0.94}Al_{0.10})O_3$ and $(Mg_{0.92}Fe_{0.09})SiO_3$ samples show a broad crossover, and the non-vanishing satellite peak in the XES spectra measured at 100 GPa was attributed to the existence of IS iron. These XES spectra, however, show great resemblance with that in Catalli *et al*. (2010), where only Fe^{3+} is present. Indeed XES shows the decrease of average electron spin moment of iron, but it shows neither which type of iron undergoes spin-state crossover, nor the exact spin state. Similarly, the spin state of iron cannot be easily determined via XANES spectra (Narygina *et al*., 2009) unambiguously.

Mössbauer spectroscopy, on the other hand, probes the nuclear quadrupole splitting (QS) caused by the interaction between nuclear quadrupole moment and the static electric potential resulting from surrounding electrons. It can be expected that QS can be sensitive to spin state, as different spin states have different d orbital occupancy, which leads to different electron charge distribution. However, it is still very difficult to identify the iron spin state solely based on the numerical value of QS. Therefore, interpretation of Mössbauer spectra can still be very ambiguous. For samples that contain mostly ferrous iron (Jackson *et al*., 2005; McCammon *et al*., 2008), a change of QS from ~2.4 to 3.5 mm/s occurring at 30 GPa has been observed, but was interpreted differently. The state with high QS (3.5 mm/s) emerging at pressures higher than 30 GPa was interpreted as IS by McCammon *et al*. (2008) and Lin *et al*. (2008), while Jackson *et al*. (2005) suggest it to be HS. The low concentration of ferric iron in Jackson *et al*. (2005) and McCammon *et al*. (2008) exhibited an increase in QS with pressure, which suggests a crossover from HS ($S = 5/2$) to LS ($S = 1/2$) state in the pressure range of 30–70 GPa. In contrast, in Al-bearing samples (Li *et al*., 2006), where ferric iron occupies the dodecahedral (A) site, the QS

remains unchanged up to 100 GPa, which suggests the A-site iron remains in the HS state. These results indicate that the ferric iron at the octahedral (B) site undergoes a spin-state crossover. Combined Mössbauer, XES, and XRD studies using samples containing equal amounts of Fe^{3+} in A and B sites supports such a mechanism: about half of the HS iron changes to LS state in the 45–60 GPa range while the other half remain in the HS state all the way to 150 GPa (Catalli *et al*., 2010).

In an attempt to better understand the spin-state crossover in perovskite and interpret experimental data, several calculations have been performed, but they are not always in agreement with each other (Lin *et al*., 2005; Hofmeister, 2006; Zhang & Oganov, 2006; Stackhouse *et al*., 2007; Bengtson *et al*., 2008, 2009; Umemoto *et al*., 2008; Hsu *et al*., 2010b, 2009). The HS-to-LS crossover pressure in ferrous iron in $(Mg,Fe)SiO_3$ determined by static calculations strongly depends on the choice of exchange-correlation. In general, GGA gives higher transition pressure than LDA by ~50 GPa (Hofmeister, 2006; Zhang & Oganov, 2006; Stackhouse *et al*., 2007; Bengtson *et al*., 2008; Umemoto *et al*., 2008; Hsu *et al*., 2009), as has been seen in other non-strongly-correlated systems as well (Tsuchiya *et al*., 2004; Yu *et al*., 2007, 2008) (see review by Wentzcovitch *et al*., 2010). It also depends on other factors, such as the magnetic and atomic order (Umemoto *et al*., 2008), the site degeneracy of irons (Umemoto *et al*., 2010), and the inclusion of on-site Coulomb interaction, Hubbard *U* (Hsu *et al*., 2010b). In all these calculations, the HS-to-IS transition is not observed. The spin-state transition of ferric iron is also discussed in some theoretical works (Lin *et al*., 2005; Zhang & Oganov, 2006; Stackhouse *et al*., 2007). Our work, so far, has focused on aluminum-free perovskites (Umemoto *et al*., 2008, 2010; Hsu *et al*., 2010b, 2011b) namely, $(Mg_{1-x}Fe_x)SiO_3$ for ferrous iron, and $(Mg_{1-x}Fe_x)(Si_{1-x}Fe_x)O_3$ for ferric iron. In the lower mantle $x \approx 0.1$, and we set $x = 0.125$ in our calculations that are summarized below. Atomic configurations used in these works are shown in Fig. 2.

4.1. Crossover in ferrous iron

For well characterized samples, Mössbauer spectroscopy is a powerful tool to probe the change of iron spin state. The nuclear charge distribution in ^{57}Fe is not spherical. Its multipole expansion has non-vanishing high-order moments. The nuclear quadrupole moment interacts with the electric field resulting from the electrons around the nucleus. The QS is directly proportional to the product of the nuclear quadrupole moment and the electric field gradient (EFG) at the center of the nucleus (Petrilli *et al*., 1998; Chen & Yang, 2007). In $(Mg,Fe)SiO_3$ perovskite, iron substitutes for magnesium in the large 8–12 coordinated cage. As previously found for the LS state, there is more than one equilibrium site for ferrous iron in the large distorted dodecahedral site (Umemoto *et al*., 2008). HS ferrous iron is relatively larger than magnesium and remains in equilibrium in the magnesium position with

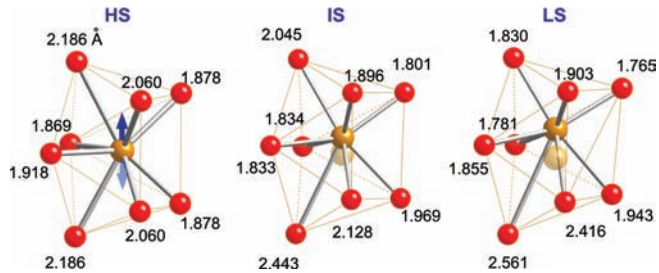

Fig. 3. Local atomic configuration around Fe^{2+} in $(Mg,Fe)SiO_3$ perovskite at 120 GPa determined using LDA (Umemoto *et al*., 2008). Yellow and red spheres represent iron and oxygen sites, respectively; numbers denote for Fe-O distances (in Å). HS Fe^{2+} resides on the high-symmetry mirror plane, while IS and LS Fe^{2+} deviate from it. Such phenomenon can be observed in the entire 0–150 GPa pressure range, regardless of the exchange-correlation functional and the inclusion of Hubbard *U*.

~8 neighbors. LS iron is smaller (Tsuchiya *et al*., 2006) and it is in unstable equilibrium in the magnesium position. Its equilibrium position is displaced vertically and has ~6 nearest neighbors (see Fig. 3) (Umemoto *et al*., 2008). It is conceivable that HS iron might also find metastable sites, in addition to the lowest energy site, within the large Mg cage. At each site, the ligand field (and electron charge distribution) is different. Such a difference, even if small, can cause significant differences in the EFG and thus lead to very different QSs, irrespective of spin state. Therefore, interpretation of the spin state on the basis of QSs observed in Mössbauer spectra is not unambiguous. At different equilibrium sites, iron in the same spin state may still have different QS.

Equilibrium sites for iron in the perovskite cage were found by following unstable vibrational modes of a hypothetical cubic perovskite structure of $(Mg_{0.75}Fe_{0.25})SiO_3$ with 20 atoms per unit cell. This structure is unstable and has several zone center modes with imaginary frequencies. Atoms were displaced according to these modes and the structure subsequently relaxed. This process was repeated until no more unstable phonons could be identified. Several metastable configurations for ferrous iron in the perovskite cage could then be found, each one with distinct QS. Work by Bengtson *et al*. (2009) also demonstrated the presence of more than one site for iron and the dependence of QS on the iron site. As shown in Umemoto *et al*. (2008), the GGA equilibrium volume of HS $(Mg_{0.75}Fe_{0.25})SiO_3$ is 286.24 a.u.3/f.u. (1144.97 a.u.3 per 20-atom cell). A hypothetical cubic perovskite cell with equal volume was generated, and its phonon frequencies and zone center normal modes were calculated. Among its seven distinct soft modes, three of them can lead to stable perovskite structures, directly or indirectly. Two of them are energetically competitive at 0 GPa and they are shown in Fig. 4.

The LS states are also obtained following the same procedure in cubic LS $(Mg_{0.75}Fe_{0.25})SiO_3$ (unit-cell volume 1137.75 a.u.^{3}). In this case none of the soft phonon modes can directly produce the final equilibrium structures with LS iron. Successive calculations of unstable phonon

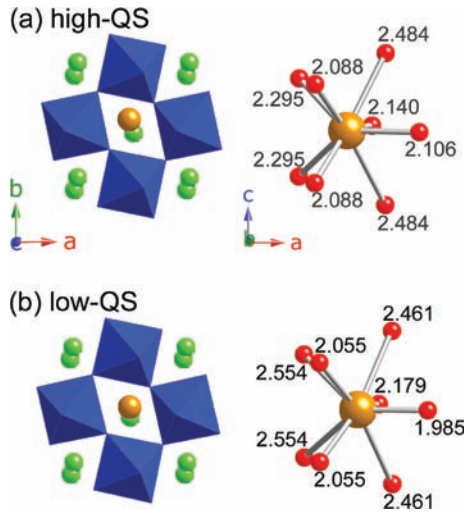

Fig. 4. Local environment of (a) high-QS and (b) low-QS HS Fe^{2+}. The numbers denote for Fe-O distances (in Å). [Figure generated from Hsu *et al*. (2010b)]

frequencies and structural relaxations produce three structures, only one of which could compete energetically with the other two HS structures (Hsu *et al.* 2010). This LS structure is the same as that found by Umemoto *et al*. (2008) and shown in Fig. 3.

The approach to find stable IS iron sites in perovskite was different. IS iron cannot be stabilized in the hypothetical cubic perovskite, and this hinders the phonon calculation. Iron was displaced from the HS equilibrium sites along the [001] direction ($P1$ symmetry) and structural optimization was performed subsequently. The atomic structures of the two competing HS states were used as the starting configuration, and the same IS site was obtained. The magnetic moment of iron can be stabilized as $S = 1$ spontaneously without applying any constraint when $P \geq 30$ GPa. Therefore, results for IS irons are reported only above 30 GPa. The atomic structure of the IS state presented in this manuscript is the same as the one presented in Umemoto *et al*. (2010).

As mentioned earlier, the QS of iron nucleus is determined by the electron charge distribution around the nucleus, not by the spin state. The ligand fields around both HS iron sites differ because of the different Fe–O arrangements shown in Fig. 3 and 4. These determine d-orbital occupancies of iron and their respective EFGs. For 40 atom cells with composition $(Mg_{0.875}Si_{0.125})SiO_3$, competing HS states at 0 GPa are semiconducting with energy gaps slightly larger than 0.1 eV. The difference in their electronic structures shows up clearly in PDOS of iron. The spin-up electrons in HS-iron occupy all five d-orbitals, and their contribution to the EFG is negligible since their charge distribution is spherical. It is the spin-down electron density that is responsible for the resulting EFG. The main EFG component, V_{zz}, depends on the orbital occupancy based on $V_{zz} \propto e\left(2n_{xy} - n_{yz} - n_{xz} - 2n_{z^2} + 2n_{x^2-y^2}\right)/r^3$ (Chen & Yang, 2007), where n_{xy}, n_{yz}, . . . , denote for the occupancy of orbitals d_{xy}, d_{yz}, . . . , respectively, and they can be calculated by integrating PDOS over energy. This expression for V_{zz} shows that electrons occupying d_{xz} or d_{yz} orbitals contribute half as much as the d_{xy}, $d_{x^2-y^2}$, or d_{z^2} electrons to the EFG. The spin-down occupancies in the HS iron with QS of 3.4 mm/s are $n_{x^2-y^2} \approx 0,47$ and $n_{xy} \approx 0.62$, while the HS iron with QS of 2.3 mm/s has spin-down $n_{yz} \approx 0.97$. The other orbitals have negligible occupancies. This origin of the different QSs of the HS iron at different sites is this difference in the d-orbital occupancy. Fig. 5 shows a summary of calculated QSs of both HS states and the lowest energy IS and LS states at lower-mantle pressures compared with experimental data.

The relative enthalpy of these states *versus* pressure in $(Mg_{0.875}Si_{0.125})SiO_3$ computed using GGA and GGA + U are shown in Fig. 6. Only the two competitive HS states, the lowest enthalpy LS state and the single IS states are included in this comparison. *These states will be referred as the low-QS (2.3 mm/s) and high-QS (3.4 mm/s) HS states, LS, and IS states in the rest of the paper*. Despite the dependence of the crossover pressure on the exchange and correlation functional, it is clear that the only crossover observed is between the low- and high-QS states at pressures similar to those observed in Mössbauer experiments (McCammon *et al*., 2008; Lin *et al*., 2008). No other crossover is obtained at mantle pressures, *i.e*. below 135 GPa. LDA and LDA+U also confirm the crossover between low- and high-QS states at low pressures. LDA also gives a HS to LS crossover at $\sim$ 100 GPa (Bengtson *et al*., 2008; Hsu *et al*., 2010b; Umemoto *et al*., 2010). However, the latter is an unrealistically low pressure and LDA +U raises this transition pressure to well beyond mantle pressures (Hsu *et al.* 2010b). Since there is no spin change associated with the change in QS observed in Mössbauer spectra, there is no significant iron polyhedral volume change and

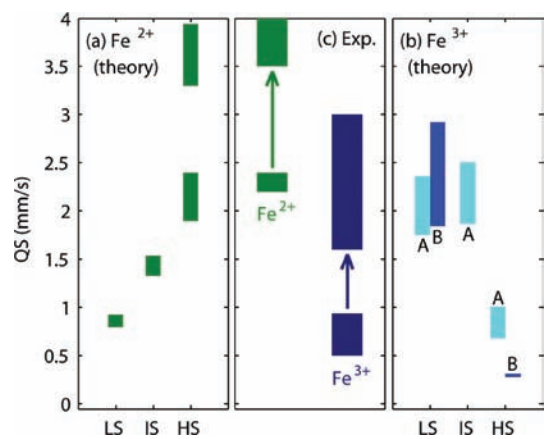

Fig. 5. Calculated quadrupole splittings of (a) ferrous iron and (b) ferric iron in $MgSiO_3$ perovskite. Letters A and B in (b) refer to iron-occupying site. The results on ferrous iron are consistent with results by Bengtson *et al*. (2009). The range of values reflects the effect of pressure in the experimentally observed range for such states and the uncertainty in the value of the nuclear quadrupole moment of iron, Q. Arrows in (c) indicate the measured effect of pressure on QSs. [Figure cited from Hsu *et al*. (2011b), in which the measured QSs are cited from Jackson *et al*. (2005); McCammon *et al*. (2008) and Catalli *et al*. (2010)]

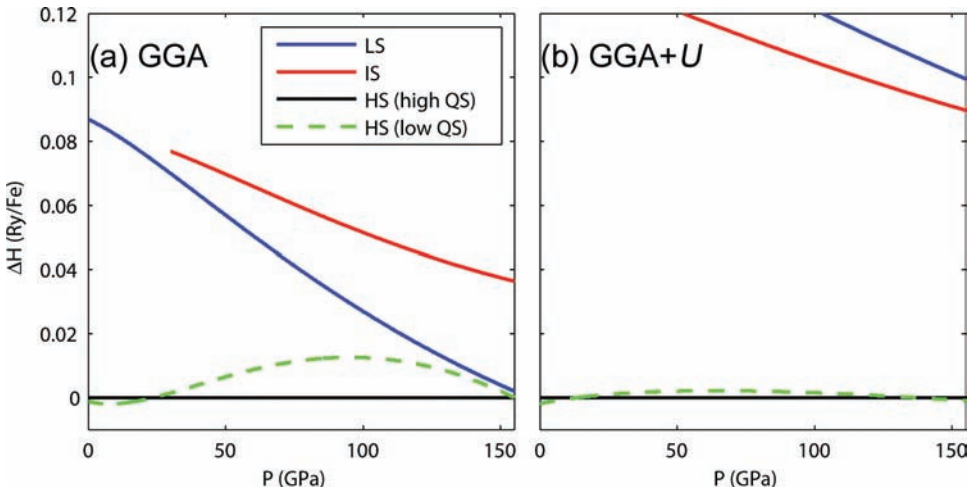

Fig. 6. Relative enthalpy of $(Mg_{1-x}Fe_x)SiO_3$ ($x = 0.125$) in each spin state determined using GGA (a) and GGA+U (b) method. The high-QS HS state is used as a reference. No spin-state crossover is observed in the lower-mantle pressure range. The only crossover is from low-QS HS to high-QS HS state. [Figure cited from Hsu *et al*. (2010b)]

no bulk modulus anomaly as observed in ferropericlase (Tsuchiya *et al*., 2006; Wentzcovitch *et al*., 2009).

4.2. Crossover in ferric iron

As to ferric iron in perovskite, possibly more abundant than ferrous iron (Fe^{3+}/Σ Fe might be as high as 2/3) (McCammon, 1997; Frost *et al*., 2004), its spin-state crossover has remained unclear since 2004. Experiments in aluminum-free iron-bearing perovskite focused mostly on ferrous iron (Jackson *et al*., 2005; Lin *et al*., 2008; McCammon *et al*., 2008). It was still observed that a low concentration of ferric iron in these sample exhibited an increase in QS with pressure, which suggests a crossover from the HS ($S = 5/2$) to LS ($S = 1/2$) state in the pressure range of 30–70 GPa (Jackson *et al*., 2005). In Al-bearing samples, where ferric iron occupies the dodecahedral (A) site, the QS remains unchanged up to 100 GPa, which suggests the A-site iron remains in the HS state. These results indicated that the ferric iron at the octahedral (B) site undergoes a spin-state crossover. A more recent experiment using $(Mg_{1-x}Fe_x)(Si_{1-x}Fe_x)O_3$ ($x = 0.1$) samples supports such a mechanism: about half of the HS iron changes to LS state in the 45–60 GPa range while the other half remains in the HS state all the way to 150 GPa (Catalli *et al*., 2010). Early computational studies on $(Mg_{1-x}Fe_x)(Si_{1-x}Fe_x)O_3$ found a ground state with HS iron at the A site and LS iron at the B site (A HS, B LS) and an A-site HS-LS crossover that leads both A- and B-site iron to a final LS state (A LS, B LS) at high pressures (Zhang & Oganov, 2006; Stackhouse *et al*., 2007). These predictions are inconsistent with experiments in two ways: (1) the predicted transition pressure was too high (>75 GPa) and (2) the predicted final HS iron concentration is too low.

We stabilized $(Mg_{1-x}Fe_x)(Si_{1-x}Fe_x)O_3$ with $x = 0.125$ in all possible spin states using a 40-atom super-cell shown in Fig. 2b (Hsu *et al*., 2011b). We also calculated the electric field gradient at the iron nucleus for all spin states. These states were also independently confirmed *via* the augmented plane-wave plus local orbitals (APW + lo) method (Madsen *et al*., 2001) implemented in the WIEN2k code (Blaha *et al*., 2001), with which the EFGs were calculated. The EFGs were converted to QSs with ^{57}Fe nuclear quadrupole moment $Q = 0.16$ (Petrilli *et al*., 1998) and 0.18 to estimate the effect of the uncertainty on the value of Q. To treat $(Mg_{1-x}Fe_x)(Si_{1-x}Fe_x)O_3$, the density functional theory plus Hubbard U (DFT + U) method is necessary, as standard DFT exchange-correlation functionals, the local density approximation (LDA) and generalized gradient approximation (GGA) lead to unwanted metallic states (especially at high pressures), in which the iron spin states are not well defined.

Within DFT+U, several combinations of iron spin states can be stabilized. The A-site ferric iron can be stabilized in HS, IS, and LS states. The B-site ferric iron can be stabilized not only in LS state, but also in the HS state that was not found in previous calculations (Zhang & Oganov, 2006; Stackhouse *et al*., 2007). The spin moments of the A- and B-site iron can be either parallel or antiparallel. The self-consistent U, U_{sc}, depends mainly on the iron spin state, slightly depends on the occupied site, and barely depends on pressure and alignment of spin moments. The relative enthalpy of each stabilized state is shown in Fig. 7, where the previously perceived ground state (A HS, B LS) is used as a reference. As can be seen, the actual ground state at low pressures is (A HS, B HS), whether using LDA + U_{sc}, GGA + U_{sc}, or using a unique constant U for all states. The crossover pressure predicted by LDA + U_{sc} best agrees with the transition pressure observed in Mössbauer spectra: 50–60 GPa (Catalli *et al*., 2010).

The calculated QSs of ferric iron (A and B site) in various spin states, along with the measured QSs (Jackson *et al*., 2005, McCammon *et al*., 2008; Catalli *et al*., 2010), are shown in blue in Fig. 5. Clearly, our calculations on ferrous and ferric iron in perovskite are consistent with Mössbauer

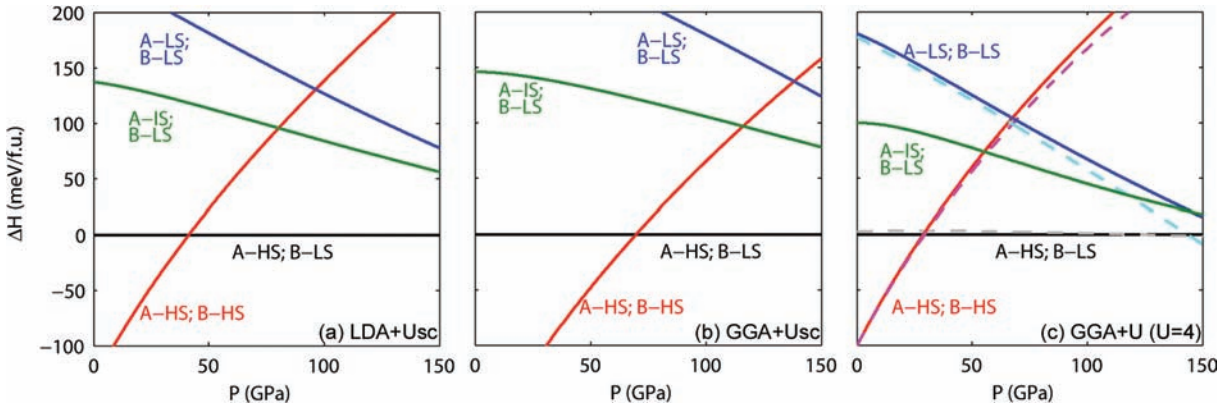

Fig. 7. Relative enthalpies of $(Mg_{1-x}Fe_x)(Si_{1-x}Fe_x)O_3$ ($x = 0.125$) in different spin states obtained using different functionals and Hubbard U. The reference state has HS iron at the A site and LS iron at the B site (A-HS; B-LS). Predicted transition pressures by LDA+U_{sc} (a), GGA+U_{sc} (b), and GGA+U with $U = 4$ eV (c) are 41, 70, and 29 GPa, respectively. Dashed lines in (c) correspond to anti-parallel spins at A and B sites. [Figure cited from Hsu *et al*. (2011b)]

spectra. The HS-LS crossover in the B-site ferric iron also helps to explain the decrease in XES satellite peak ($K\beta$) intensity (Badro *et al*., 2004; Li *et al*., 2004). The QS of ferrous and ferric iron exhibit exactly the opposite trends with respect to the spin moment. This can be understood *via* their orbital occupancies. The LS ferrous iron, although occupying the A site, is effectively located near the center of a Fe-O octahedron, as it is vertically displaced from the mirror plane (Umemoto *et al*., 2008). Its six 3*d* electrons doubly occupy the three orbitals with t_{2g} character and form a charge density with cubic-like shape, which barely contributes to the EFG and leads to a very small QS. The HS ferric iron also has a small EFG (and thus QS), irrespective of A or B site. This is because its five 3*d* electrons (all spin-up) occupy all 3*d* orbitals, forming an almost spherically shaped electron charge distribution that leads to a small EFG (and thus QS). Similarly, the spin-up electrons in HS ferrous and LS ferric iron barely contribute to EFG, as their charge distributions are nearly spherical and cubic, respectively. It is their spin-down electrons that contribute to the EFGs and lead to larger QSs. This is why the spin moments of ferrous and ferric iron appear to affect the QSs in an opposite manner.

The LDA+U_{sc} compression curves and bulk modulus ($K = VdP/dV$) of $(Mg_{1-x}Fe_x)(Si_{1-x}Fe_x)O_3$ perovskite ($x = 0.125$) along with the experimental data ($x = 0.1$) (Catalli *et al*., 2010) are shown in Fig. 7. At low pressures (<45 GPa), the experimental data fall on the calculated compression curve corresponding to the (A-HS, B-HS) state. Starting from ~45 GPa, the data points deviate from the (A-HS, B-HS) curve and then join the (A-HS, B-LS) curve at ~60 GPa. Starting from ~90 GPa, the data deviate from the curve again. This, however, is very likely to result from the questionable accuracy of the Au pressure scale used in the experiment, as in the case of $(Mg_{1-x}Fe_x)SiO_3$ perovskite (Hsu *et al*., 2010b). The observed volume reduction shown in Fig. 8a further confirms the B-site HS-LS crossover, as seen in ferropericlase (Lin *et al*., 2005; Tsuchiya *et al*., 2006).

At finite temperatures, the spin-state crossover passes through a mixed-spin (MS) state (namely, HS and LS coexist) within a finite pressure range that increases with temperature. During the crossover, the thermodynamic properties of the MS state exhibit anomalous behavior that may affect mantle properties. One example is the softening in bulk modules and its effect on the compressional wave velocity, as already observed in ferropericlase (Crowhurst *et al*., 2008; Wentzcovitch *et al*., 2009; Wu *et al*., 2009). To estimate such anomaly in $(Mg_{1-x}Fe_x)(Si_{1-x}Fe_x)O_3$ perovskite, we employed the thermodynamic model described in section 3.2 and used to describe ferropericlase (Wentzcovitch *et al*., 2009; Wu *et al*., 2009). Here, we do not include vibrational free energy, as it barely affects the magnitude of the anomaly, slightly increases the transition pressure, and uniformly decreases the bulk modulus. The calculated $V(P)$ curve of $(Mg_{1-x}Fe_x)(Si_{1-x}Fe_x)O_3$ perovskite in the MS state (using LDA+U_{sc}) at room temperature (300 K), shown as the dashed line in Fig. 8a, exhibits a volume reduction (~1.2 %) around the predicted transition pressure, 41 GPa. This reduction leads to a significant softening in bulk modulus, as shown in Fig. 8b. The softening is still prominent at 2000 K, the temperature near the top of the lower mantle (~660 km deep). Given the abundance of iron-bearing perovskite and the possibly high population of ferric iron, this softening may have a noticeable impact on the mantle properties, including possible anomalies in the seismic wave velocities.

5. Summary

First-principles calculations of iron-bearing perovskite are able to reproduce experimental data and are shown to be essential for their interpretation, as experimental methods used to investigate pressure-induced spin state changes, *i.e*. Mössbauer spectroscopy and XES, cannot unambiguously identify iron spin states. The main conclusions reached in this work are:

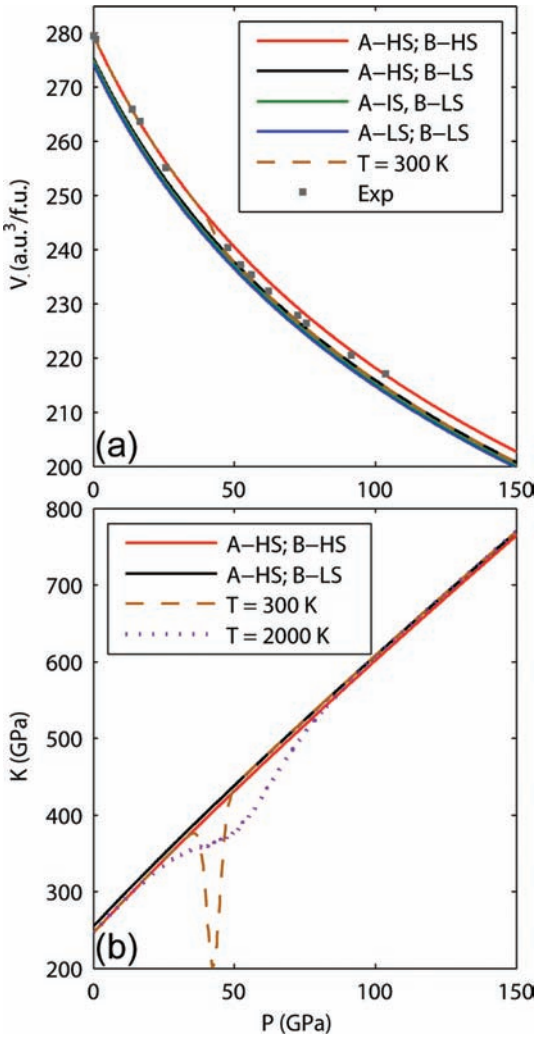

Fig. 8. (a) Compression curves and (b) bulk modulus of $(Mg_{1-x}, Fe_x)(Si_{1-x}, Fe_x)O_3$ ($x = 0.125$) Pv computed with LDA+U_{sc} and room-temperature measurements ($x = 0.1$). Both the measured and calculated compression curves exhibit a clear reduction accompanying the B-site HS-LS crossover, which leads to a softening in bulk modulus shown in (b). [Figure cited from Hsu *et al*. (2011b); room-temperature measurements cited from Catalli *et al*. (2010).]

(1) There is no spin crossover in ferrous iron in the A site of the perovskite structure within the pressure range of the mantle. A lateral displacement of HS ferrous iron on the *a-b* plane produces an HS state with higher Mössbauer QS (~3.5 mm/s) seen at ~ 30 GPa. This change does not produce volume elastic anomalies. Ferrous iron in the LS and IS states in the A site are displaced along [001]. They are ''smaller'' cations and shift to sites with six nearest neighbors only. These states are not energetically competitive at mantle pressures.

(2) Only ferric iron at the B-site undergoes HS-LS crossover. This takes place at ~ 50–60 GPa and produces a volume change of ~ 1 %. There is no HS-LS crossover in the A site. IS and LS states are not energetically competitive at mantle pressures. Even if the A-site Fe^{3+} did undergo a spin crossover, it would not lead to anomaly in bulk modulus, as the spin state of A-site Fe^{3+} barely affects the compression curve.

(3) Ferric iron should affect mantle properties more significantly than ferrous iron because of its crossover and its expected abundance.

The real mantle perovskite, $(Mg,Fe,Al)(Si,Al,Fe)O_3$, contains also ~ 5 % of aluminum and the microscopic state of this system under the high pressures and temperatures of the mantle is still quite uncertain. Recent Mössbauer experiments (Catalli *et al*., 2011) see a change in iron nuclear QS starting at 70 GPa, accompanied by a density anomaly. This has been attributed to the presence of ferric iron in the B site. This interpretation is consistent with results reported above, but calculations still need to confirm the microscopic picture in aluminum-bearing perovskite. The real challenge is to describe the microscopic state of $(Mg,Fe,Al)(Si,Al,Fe)O_3$ at the high temperatures of the mantle.

Acknowledgement: We thank Peter Blaha for his calculations of quadrupole splittings and valuable discussions in this series of works, Matteo Cococcioni for his assistance with the DFT+ *U* method, and Sergio Speziale for helpful comments on the manuscript. This work was primarily supported by the MRSEC Program of NSF under Grants No. DMR-0212302 and No. DMR-0819885, and partially supported by EAR-081272, EAR-1047629, and ATM-0426757 (***VLab***). Calculations were performed at the Minnesota Supercomputing Institute (MSI).

References

Badro, J., Fiquet, G., Guyot, F., Rueff, J.P., Struzhkin, V.V., Vanko, G., Monaco, G. (2003): Iron partitioning in Earth's mantle: toward a deep lower mantle discontinuity. *Science*, **300**, 789–791.

Badro, J., Rueff, J.P., Vanko, G., Monaco, G., Fiquet, G., Guyot, F. (2004): Electronic transitions in perovskite: possible non-convecting layers in the lower mantle. *Science*, **305**, 383–386.

Baroni, S., de Gironcoli, S., Dal Corso, A., Giannozzi, P. (2001): Phonons and related crystal properties from density-functional perturbation theory. *Rev. Mod. Phys.*, **73**, 515–562.

Bengtson, A., Persson, K., Morgan, D. (2008): *Ab initio* study of the composition dependence of the pressure-induced spin crossover in perovskite $(Mg_{1-x},Fe_x)SiO_3$. *Earth Planet. Sc. Lett.*, **265**, 535–545.

Bengtson, A., Li, J., Morgan, D. (2009): Mössbauer modeling to interpret the spin sate of iron in $(Mg,Fe)SiO_3$. *Geophys. Res. Lett.*, **36**, L15301.

Blaha, P., Schwarz, K., Madsen, G.K.H., Kvasnicka, D., Luitz, J. (2001): WIEN2k, An Augmented plane wave+local orbitals program for calculating crystal properties, edited by K. Schwarz, Technical Universität Wien, Vienna.

Bower, D.J., Gurnis, M., Jackson, J.M., Sturhahn, W. (2009): Enhanced convection and fast plumes in the lower mantle

induced by the spin transition in ferropericlase. *Geophys. Res. Lett.*, **36**, L10306–1–4.

Catalli, K., Shim, S.-H., Prakapenka, V.B., Zhao, J., Sturhahn, W., Chow, P., Xiao, Y., Liu, H., Cynn, H., Evans, W.J. (2010): Spin state of ferric iron in $MgSiO_3$ perovskite and its effect on elastic properties. *Earth Planet. Sci. Lett.*, **289**, 68–75.

Catalli, K., Shim, S.-H., Prakapenka, V.B., Zhao, J., Sturhahn, W., Chow, P., Xiao, Y., Cynn, H., Evans, W.J. (2011): Effects of the Fe^{3+} spin transition on the properties of aluminous perovskite - New insights for lower-mantle seismic heterogeneities. *Earth Planet. Sci. Lett.*, **310**, 293–302.

Ceperley, D.M. & Alder, B.J. (1980): Ground state of the electron gas by a stochastic method. *Phys. Rev. Lett.*, **45**, 566–569.

Chen, Y.L. & Yang, D.P. (2007): Mössbauer effect in Lattice dynamics. Wiley-VCH, Weinheim.

Cococcioni, M. (2010): Accurate and efficient calculations on strongly correlated minerals with the LDA+ *U* method: review and perspectives. *Rev. Mineral. Geochem.*, **71**, 147–167.

Cococcioni, M. & de Gironcoli, S. (2005): Linear response approach to the calculation of the effective interaction parameters in the LDA+*U* method. *Phys. Rev. B*, **71**, 035105–1–16.

Cohen, R.E., Mazin, I.I., Isaak, D.G. (1997): Magnetic collapse in transition metal oxides at high pressure: implications for the Earth. *Science*, **275**, 654–657.

Crowhurst, J., Brown, J.M., Goncharov, A., Jacobsen, S.D. (2008): Elasticity of (Mg,Fe)O through the spin transition of iron in the lower mantle. *Science*, **319**, 451–453.

Fabris, S., de Gironcoli, S., Baroni, S., Vicario, G., Balducci, G. (2005): Taming multiple valence with density functionals: a case study of defective ceria. *Phys. Rev. B*, **71**, 041102–1–4.

Fjellvag, H., Gronvold, S., Stolen, S., Hauback, B. (1996): On the crystallographic and magnetic structures of nearly stoichiometric iron monoxide. *J. Sol. St. Chem.*, **124**, 52–57.

Frost, D.J., Liebske, C., Langenhorst, F., McCammon, C., Trønnes, R., Rubie, D. (2004): Experimental evidence for the existence of iron-rich metal in the Earth's lower mantle. *Nature*, **428**, 409–412.

Fyfe, W.S. (1960): The possibility of d-electron uncoupling in olivine at high pressures. *Geochim. Cosmochim. Acta*, **19**, 141–143.

Gaffney, E.S. & Anderson, D.L. (1973): Effect of low-spin Fe^{2+} in the composition of the lower mantle. *J. Geophys. Res.*, **78**, 7005–7014.

Giannozzi, P. *et al*. (2009): QUANTUM ESPRESSO: a modular and open-source software project for quantum simulations of materials. *J. Phys. Condens. Matter*, **21**, 395502–1–39.

Grocholski, B., Shim, S.H., Sturhahn, W., Zhao, J., Xiao, Y., Chow, P.C. (2009): Spin and valence states of iron in $(Mg_{0.8}Fe_{0.2})SiO_3$ perovskite. *Geophys. Res. Lett.*, **36**, L24303.

Hofmeister, A.M. (2006): Is low-spin Fe^{2+} present in Earth's mantle? *Earth Planet. Sc. Lett.*, **243**, 44–52.

Hohenberg, P. & Kohn, W. (1964): Inhomogeneous electron gas. *Phys. Rev.*, **136**, B864–871.

Hsu, H., Umemoto, K., Cococcioni, M., Wentzcovitch, R.M. (2009): First-principles study for low-spin $LaCoO_3$ with structurally consistent Hubbard. *U. Phys. Rev. B*, **79**, 125124–1–9.

Hsu, H., Umemoto, K., Wu, Z., Wentzcovitch, R.M. (2010a): Spin-state crossover of iron in lower-mantle minerals: results of DFT+*U* investigations. *Rev. Mineral. Geochem.*, **71**, 169–199.

Hsu, H., Umemoto, K., Blaha, P., Wentzcovitch, R.M. (2010b): Spin states and hyperfine interactions of iron in $(Mg,Fe)SiO_3$ perovskite under pressure. *Earth Planet. Sci. Lett.*, **294**, 19–26.

Hsu, H., Blaha, P., Wentzcovitch, R.M., Leighton, C. (2010c): Cobalt spin states and hyperfine interactions in $LaCoO_3$ investigated by LDA+*U* calculations. *Phys. Rev. B (Rapid Comm.)*, **82**, 100406R–1–4.

Hsu, H., Umemoto, K., Wentzcovitch, R.M., Cococcioni, M. (2011a): The Hubbard *U* correction in iron bearing minerals: a discussion based on $(Mg,Fe)SiO_3$ perovskite. *Phys. Earth Planet. Int.*, **185**, 13–19.

Hsu, H., Blaha, P., Cococcioni, M., Wentzcovitch, R.M. (2011b): Spin-state crossover and hyperfine interactions of ferric iron in $MgSiO_3$ perovskite. *Phys. Rev. Lett.*, **106**, 118501–1–4.

Irifune, T., Shinmei, T., McCammon, C.A., Miyajima, N., Rubie, D.C., Frost, D.J. (2010): Iron partitioning and density changes of pyrolite in Earth's lower mantle. *Science*, **327**, 193–195.

Jackson, J.M., Sturhahn, W., Shen, G., Zhao, J., Hu, M.Y., Errandonea, D., Bass, J.D., Fei, Y. (2005): A synchrotron Mössbauer spectroscopy study of $(Mg,Fe)SiO_3$ perovskite up to 120 GPa. *Am. Mineral.*, **90**, 199–205.

Kiefer, B., Stixrude, L., Wentzcovitch, R.M. (2002): Elasticity of $(Mg,Fe)SiO_3$-perovskite at lower mantle conditions. *Geophys. Res. Lett.*, **29**, 34–1–4.

Kohn, W. & Sham, L.J. (1965): Self-consistent equations including exchange and correlation effects. *Phys. Rev.*, **140**, A1133–1138.

Li, J., Struzhkin, V., Mao, H., Shu, J., Memeley, R., Fei, Y., Mysen, B., Dera, P., Pralapenka, V., Shen, G. (2004): Electronic post spin state of iron in lower mantle perovskite. *Proc. Natl. Acad. Sc. USA*, **101**, 14027–14030.

Li, J., Sturhahn, W., Jackson, J.M., Struzhkin, V.V., Lin, J.F., Zhao, J., Mao, H.K., Shen, G. (2006): Pressure effect on the electronic structure of iron in $(Mg,Fe)(Si,Al)O_3$ perovskite: a combined synchrotron Mössbauer and X-ray emission spectroscopy study up to 100 GPa. *Phys. Chem. Minerals*, **33**, 575–585.

Lin, J.F. & Tsuchiya, T. (2008): Spin transition of iron in the earth's lower mantle. *Phys. Earth Planet. Inter.*, **170**, 248–259.

Lin, J.F., Struzhkin, V.V., Jaconsen, S.D., Hu, M.Y., Chow, P., Kung, J., Liu, H., Mao, H.-K., Hemley, R. (2005): Spin transition of iron in magnesiowüstite in the Earth's lower mantle. *Nature*, **436**, 377–380.

Lin, J.F., Watson, H., Vanko, G., Alp, E.E., Prakapenka, V.B., Dera, P., Struzhkin, V., Kubo, A., Zhao, J., McCammon, C., Evans, W.J. (2008): Intermediate-spin ferrous iron in lowermost mantle post-perovskite and perovskite. *Nature Geosci.*, **1**, 688–691.

Lundin, S., Catalli, K., Santillan, J., Shim, S.H., Prakapenka, V.B., Kunz, M., Meng, Y. (2008): Effect of Fe on the equation of state of mantle silicate perovskite over 1 Mbar. *Phys. Earth Planet. Inter.*, **168**, 97–102.

Madsen, G., Blaha, P., Schwarz, K., Sjoestedt, E., Nordstroem, L. (2001): Efficient linearization of the augmented plane-wave method. *Phys. Rev. B*, **64**, 195134–1–9.

Matyska, C., Yuen, D.A., Wentzcovitch, R.M., Cizkova, H. (2011): The impact of variability in the rheological activation parameters on lower-mantle viscosity stratification and its dynamics. *Phys. Earth & Planet Int.*, **188**, 1–8.

McCammon, C. (1997): Perovskite as a possible sink for ferric iron in the lower mantle. *Nature*, **387**, 694–697.

McCammon, C., Kantor, I., Narygina, O., Rouquette, J., Ponkratz, U., Sergueev, I., Mezouar, M., Prakapenka, V., Dubrovinsky, L. (2008): Stable intermediate-spin ferrous iron in lower-mantle perovskite. *Nature Geosci.*, **1**, 684–687.

Murakami, M., Hirose., K., Kawamura, K., Sata, N., Ohishi, Y. (2004): Post-perovskite phase transition in $MgSiO_3$. *Science*, **304**, 855–858.

Murakami, M., Hirose, K., Sata, N., Ohishi, Y. (2005): Post-perovskite phase transition and mineral chemistry in the pyrolitic lowermost mantle. *Geophys. Res. Lett.*, **32**, L03304.

Narygina, O., Mattesini, M., Kantor, I., Pascarelli, S., Wu, X., Aquilanti, G., McCammon, C., Dubrovinsky, L. (2009): High-pressure experimental and computational XANES studies of $(Mg,Fe)(Si,Al)O_3$ perovskite and (Mg,Fe)O ferropericlase as in the Earth's lower mantle. *Phys. Rev. B*, **79**, 174115–1–9.

Oganov, A.R. & Ono, S. (2004): Theoretical and experimental evidence for a post-perovskite phase of $MgSiO_3$ in Earth's D'' layer. *Nature*, **430**, 445–448.

Ohnishi, S. (1978): A theory of pressure-induced high-spin-low-spin transition of transition metal oxides. *Phys. Earth Planet. Inter.*, **17**, 130–139.

Perdew, J.P. & Zunger, A. (1981): Self-interaction correction to density-functional approximations for many-electron systems. *Phys. Rev. B*, **23**, 5048–5079.

Perdew, J.P., Burke, K., Ernzerhof, M. (1996): Generalized gradient approximation made simple. *Phys. Rev. Lett.*, **77**, 3865–3868.

Petrilli, H.M., Blöchl, P.E., Blaha, P., Schwarz, K. (1998): Electric-field-gradient calculations using the projector augmented wave method. *Phys. Rev. B*, **57**, 14690–14697.

Ringwood, A.E. (1982): Phase transformations and differentiation in subducted lithosphere: implications for mantle dynamics basalt petrogenesis and crustal evolution. *J. Geol.*, **90**, 611–642.

Rollmann, G., Rohrbach, A., Entel, P., Hafner, J. (2004): First-principles calculation of the structure and magnetic phases of hematite. *Phys. Rev. B*, **69**, 165107.

Shahnas, M.H., Peltier, W.R., Wu, Z., Wentzcovitch, R.M. (2011): The high pressure electronic spin transition in iron: potential impacts upon mantle mixing. *J. Geophys. Res.*, **116**, B08205–1–16.

Sherman, D.M. (1988): High-spin to low-spin transition of iron(II) oxides at high pressures: possible effects on the physics and chemistry of the lower mantle. *In* ''Structural and Magnetic Phase Transition in Minerals'', S. Ghose, J.M.D. Coey, E. Salje eds. Springer Verlag, New York, 113–118.

Sherman, D.M. (1991): The high-pressure electronic structure of magnesiowüstite (Mg,Fe)O: applications to the physics and chemistry of the lower mantle. *J. Geophys. Res.*, **96**, 14299–14312.

Sherman, D.M. & Jansen, H.J.F. (1995): First-principles predictions of the high-pressure phase transition and electronic structure of FeO: implications for the chemistry of the lower mantle and core. *Geophys. Res. Lett.*, **22**, 1001–1004.

Stackhouse, S., Brodolt, J.P., Price, G.D. (2007): Electronic spin transitions in iron-bearing $MgSiO_3$ perovskite. *Earth Planet Sci. Lett.*, **253**, 282–290.

Tsuchiya, T., Tsuchiya, J., Umemoto, K., Wentzcovitch, R.M. (2004): Phase transition in $MgSiO_3$ perovskite in the Earth's lower mantle. *Earth Planet. Sci. Lett*, **224**, 241–248.

Tsuchiya, T., Wentzcovitch, R.M., da Silva, C.R.S., de Gironcoli, S. (2006): Spin transition in magnesiowüstite in earth's lower mantle. *Phys. Rev. Lett.*, **96**, 198501–1–4.

Umemoto, K., Wentzcovitch, R.M., Yu, Y.G., Requist, R. (2008): Spin transition in $(Mg,Fe)SiO_3$ perovskite under pressure. *Earth Planet. Sci. Lett.*, **276**, 198–206.

Umemoto, K., Hsu, H., Wentzcovitch, R.M. (2010): Effect of site degeneracies on the spin crossover in $(Mg,Fe)SiO_3$ perovskite. *Phys. Earth Planet. Inter.*, **180**, 209–214.

Vanderbilt, D. (1990): Soft self-consistent pseudopotentials in a generalized eigenvalue formalism. *Phys. Rev. B*, **41**, R7892–7895.

Wallace, D. (1972): Thermodynamics of crystals. Wiley, New York.

Wentzcovitch, R.M., Martins, J.L., Price, G.D. (1993): Ab initio molecular dynamics with variable cell shape: application to $MgSiO_3$. *Phys. Rev. Lett.*, **70**, 3947–3950.

Wentzcovitch, R.M., Tsuchiya, T., Tsuchiya, J. (2006): $MgSiO_3$ postperovskite at D'' conditions. *Proc. Natl. Acad. Sci. USA*, **103**, 543–546.

Wentzcovitch, R.M., Justo, J.F., Wu, Z., da Silva, C.R.S., Yuen, D.A., Kohlstedt, D. (2009): Anomalous compressibility of ferropericlase throughout the iron spin cross-over. *Proc. Natl. Acad. Sci. USA*, **106**, 8447–8452.

Wentzcovitch, R.M., Yu, Y., Wu, Z. (2010): Thermodynamic properties and phase relations in mantle minerals by first principles quasiharmonic theory. *Rev. Mineral. Geochem.*, **71**, 59–98.

Wu, Z., Justo, J.F., da Silva, C.R.S., de Gironcoli, S., Wentzcovitch, R.M. (2009): Anomalous thermodynamic properties in ferropericlase throughout its spin crossover transition. *Phys. Rev. B*, **80**, 014409–1–8.

Yu, Y., Wentzcovitch, R.M., Tsuchiya, T. (2007): First-principles investigation of the postpinel transition in Mg_2SiO_4. *Geophys. Res. Lett.*, **34**, L10306–1–4.

Yu, Y., Wu, Z., Wentzcovitch, R.M. (2008): α-β-γ transformations in Mg_2SiO_4 in Earth's transition zone. *Earth Planet. Sci. Lett.*, **273**, 115–122.

Zhang, F. & Oganov, A.R. (2006): Valence state and spin transitions of iron in Earth's mantle silicates. *Earth Planet. Sci. Lett.*, **249**, 436–443.

Received 27 October 2011
Modified version received 10 July 2012
Accepted 13 July 2012